Performance of 1-THz-Bandwidth, 2-D Smoothing by Spectral Dispersion and Polarization Smoothing of High-Power, Solid-State Laser Beams

Introduction

A direct-drive inertial confinement fusion (ICF) implosion of a spherical capsule containing thermonuclear fuel is initiated by the ablation of material from the outer shell surface with overlapped, intense laser beams.[1] The ablated shell mass forms a coronal plasma that surrounds the target and accelerates the shell inward via the rocket effect.[1,2] Perturbations at the ablation surface resulting from target imperfections and laser irradiation nonuniformities (known as laser imprint) are amplified by the ablative Rayleigh–Taylor (RT) instability as the shell accelerates inward and are further amplified during the deceleration phase.[3–9] The RT instability can reduce the thermonuclear yield of the implosion.[1,2] The direct-drive ICF program strives to reduce laser imprint levels by uniform laser irradiation of the target. High-compression direct-drive experiments require a 1% rms level of the on-target laser irradiation nonuniformity averaged over a few hundred picoseconds.[10] This is accomplished on the 60-beam, 30-kJ, 351-nm OMEGA laser system[11] using two-dimensional smoothing by spectral dispersion (2-D SSD),[10,12–14] distributed phase plates (DPP's),[15,16] polarization smoothing (PS) utilizing birefringent wedges,[17–19] and multiple-beam overlap.[20] These techniques are directly applicable to direct-drive ignition target designs[21] planned for the 1.8-MJ, 351-nm, 192-beam National Ignition Facility (NIF) at the Lawrence Livermore National Laboratory.[22]

The 2-D SSD UV bandwidth ($\Delta\nu_{UV}$) on OMEGA was recently increased to 1 THz, and polarization smoothing was added through the installation of a birefringent wedge in each of the 60 beams. The amount of smoothing achieved with 1-THz, 2-D SSD and PS is reported. The experimental techniques outlined in Ref. 14 are used to determine the single-beam irradiation nonuniformity from the measured ultraviolet equivalent-target-plane (UVETP) images of laser pulses having constant intensity and varying duration. Simulations of the experimental data using the properties of the phase plates, frequency modulators, and birefringent wedges are shown to be in good agreement with the measured results.

2-D SSD and PS

Laser-beam nonuniformities can be significantly reduced for high-power/energy glass lasers using 1-THz, 2-D SSD and PS. Two-dimensional SSD reduces the single-beam irradiation nonuniformity as a function of time, while the PS provides an additional, instantaneous reduction by a factor of $\sqrt{2}$ in the on-target nonuniformity.[10] The temporal dynamics of the laser-beam smoothing with 2-D SSD and PS are illustrated in Fig. 98.1. The curves plotted in Fig. 98.1 for 0.2-THz, 2-D SSD (dashed line); 1-THz, 2-D SSD (dotted line); and 1-THz,
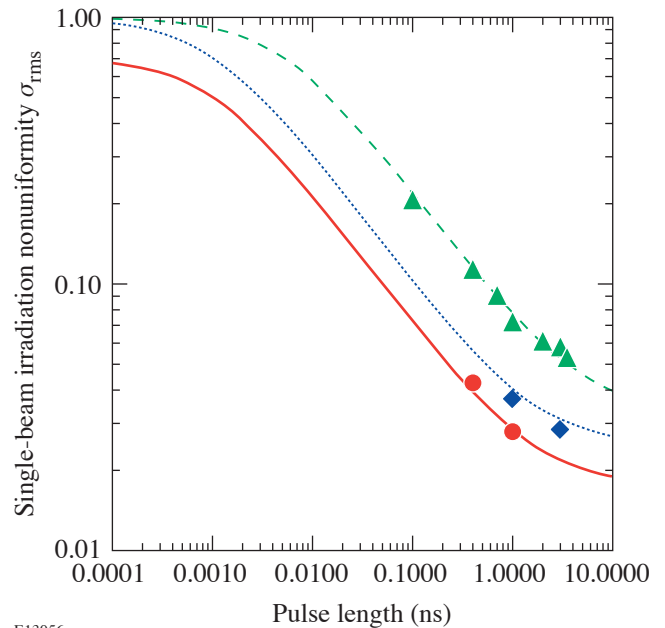
E13056

Figure 98.1

The single-beam irradiation nonuniformity σ_{rms} is plotted as a function of time for three laser-beam-smoothing conditions under consideration. Smoothing curves of the predicted σ_{rms} [see Eq. (1)] are plotted for 0.2-THz, 2-D SSD (dashed line); 1-THz, 2-D SSD (dotted line); and 1-THz, 2-D SSD with PS (solid line). The experimental results are plotted for 0.2-THz, 2-D SSD (triangles); 1-THz, 2-D SSD (diamonds); and 1-THz, 2-D SSD with PS (circles). The model shows excellent agreement with the experimental results that are a compilation of data from more than 200 laser shots. The error bars are smaller than the symbols.

2-D SSD with PS (solid line) represent the model predictions[14] for the single-beam irradiation nonuniformity σ_{rms}:

$$\sigma_{rms} = \sqrt{\sigma_0^2 \left(\frac{t_c}{t + t_c} \right) + \sigma_{asymp}^2} , \tag{1}$$

where $t_c = 1/\Delta \nu_{UV}$ is the coherence time, t is the averaging time (i.e., pulse length), σ_0 is the initial laser nonuniformity, and σ_{asymp} is the asymptotic level of smoothing with 2-D SSD and PS taken from Eq. (8) of Ref. 23. The σ_{rms} predicted with Eq. (1) has been shown to be nearly indistinguishable from the σ_{rms} predicted with the time-integrated simulation described below.[14] The model shows excellent agreement with the experimental results as discussed in the next section. The laser-beam smoothing parameters are listed in Table 98.I. As seen in Fig. 98.1, prior to reaching asymptotic levels, increasing $\Delta \nu_{UV}$ of the 2-D SSD from 0.2 THz (dashed line) to 1 THz (dotted line) reduces the amount of time needed to smooth to a given level of nonuniformity by a factor of 5. Also, for time $t \gg t_c$, it reduces the level of nonuniformity at any given time by a factor of $\sqrt{5}$. A comparison of the smoothing curve for the 1-THz, 2-D SSD (dotted line) with the curve for 1-THz, 2-D SSD with PS (solid line) shows that PS provides an instantaneous reduction in σ_{rms} by $\sqrt{2}$.

Table 98:I: Specifications for laser-beam smoothing.

2-D SSD $\Delta \nu_{UV}$ (THz)	PS	$t_c = 1/\Delta \nu_{UV}$ (ps)	σ_0	σ_{asymp}
0.2	off	5	1.00	3.30×10^{-2}
1.0	off	1	1.00	2.52×10^{-2}
1.0	on	1	0.707	1.77×10^{-2}

Laser-beam smoothing with PS is instantaneous, while 2-D SSD produces uniform far-field spots on target in a time-averaged sense. One-dimensional SSD is achieved on OMEGA by frequency modulating the phase of the laser beam, wavelength dispersing the beam using a diffraction grating, and passing the beam through a phase plate placed just before the focusing lens.[10,12] Two-dimensional SSD is achieved by applying the 1-D SSD operations in two orthogonal directions.[10] Highly reproducible spatial intensity envelopes and speckle distributions are produced in the far field. The implementation of PS on OMEGA is described elsewhere.[10] Each UV beam, polarized at 45° to the ordinary and extraordinary axes of a birefringent wedge placed before the phase plate, is split into two beams of equal intensities that refract through the wedged

surface at slightly different angles and focus on target with a separation of ~85 μm, about 37 times the beam's diffraction limited width (f number times the laser wavelength = 2.3 μm). The two beams each produce essentially the same speckle pattern on target, determined by the phase plate, but since these patterns are spatially uncorrelated with opposite polarization states, they combine through the addition of intensities rather than electric fields. This leads to the instantaneous reduction in the nonuniformity by a factor of $\sqrt{2}$.

The time-integrated far field is calculated by temporally integrating the modulus squared of a 2-D spatial Fourier transform of the UV near field. The complex-valued electric field that describes the UV near field can be written as

$$\bar{E}(x,y,t) = E_0(x,y,t)\exp\left[i\phi_{\text{2-D SSD}}(x,y,t)\right]$$

$$\cdot \exp\left[i\phi_B(x,y,t)\right] \cdot \exp\left[i\phi_{\text{DPP}}(x,y)\right]$$

$$\cdot \left\{ \hat{x} + \exp\left[i\phi_{\text{PS}}(y)\right]\hat{y} \right\}, \tag{2}$$

where $E_0(x,y,t)$ defines the temporal and spatial beam envelope, $\phi_{\text{2-D SSD}}(x,y,t)$ is the 2-D SSD phase contribution, $\phi_B(x,y,t)$ is the intensity-dependent phase contribution of the B-integral,[24] $\phi_{\text{DPP}}(x,y)$ is the static phase-plate contribution that depends on the particular phase-plate design, and $\phi_{\text{PS}}(y)$ is a linear phase term due to the birefringent wedge. The ideal spatially and temporally varying phase due to 2-D SSD can be expressed as

$$\phi_{\text{2-D SSD}}(x,y,t) \equiv 3\delta_{M_x} \sin\left[\omega_{M_x}\left(t + \xi_x x\right)\right]$$

$$+ 3\delta_{M_y} \sin\left[\omega_{M_y}\left(t + \xi_y y\right)\right], \tag{3}$$

where the x and y subscripts denote the two smoothing dimensions, $\delta_{M_{x,y}}$ is the modulation depth, $\nu_{M_{x,y}} \equiv \omega_{M_{x,y}}/2\pi$ is the RF modulation frequency, and $\xi_{x,y}$ describes the variation in phase across the beam due to the angular grating dispersion. The factor of 3 in Eq. (3) indicates that the electric field has undergone frequency tripling from the IR to UV. The 2-D SSD system parameters on OMEGA for the UVETP measurements are $\delta_{M_x} = 14.3$, $\nu_{M_x} \equiv 10.4$ GHz, $\xi_x = 0.300$ ns/m, $\delta_{M_y} = 6.15$, $\nu_{M_y} \equiv 3.30$ GHz, and $\xi_y = 1.13$ ns/m, assuming a nominal beam diameter of 27.5 cm. The modulation depths

are given for the IR. The IR bandwidths, defined as $\Delta v_x = 2\delta_{M_x} v_{M_x}$ and $\Delta v_y = 2\delta_{M_y} v_{M_y}$, correspond to $\Delta\lambda_x = 11.0$ Å and $\Delta\lambda_y = 1.50$ Å. The maximum angular spread $\Delta\theta$ is given by $\Delta\theta = \xi(c/\lambda)\Delta\lambda$, where c is the speed of light and $\lambda = 1053$ nm. B-integral effects are negligible for all cases except when the frequency modulation is turned off.[14] The linear phase term due to the birefringent wedge is

$$\phi_{PS}(y) = k_0 \sin(\Delta\theta_{PS})y,$$

where $k_0 = 2\pi/\lambda_{UV}$ is the UV laser wave number with $\lambda_{UV} = 351$ nm and $\Delta\theta_{PS} = 47$ μrad is the angular separation due to the birefringent wedge.

Experimental Results and Analysis

A description of the UVETP diagnostic used in this study can be found in Ref. 14. This diagnostic uses a full-aperture optical wedge in one of the 60 beams to direct a small fraction of the laser light to a phase plate and an OMEGA focusing lens, and it records the UVETP image on a CCD camera (see Fig. 1 of Ref. 14). The capability of the UVETP diagnostic to resolve fully individual speckles has been demonstrated.[14] Shots with PS have the birefringent wedge placed in the beam before the full-aperture optical wedge. A far-field image recorded with the UVETP diagnostic of a 1-ns square laser pulse with 1-THz, 2-D SSD and PS is presented in Fig. 98.2. The UVETP diagnostic was configured with a phase plate that produced a far-field spot with a super-Gaussian spatial-intensity envelope $\left[I \sim \exp(r/r_0)^{2.3}\right]$. The image, which has been flat fielded, shows a smooth spatial-intensity envelope [see the single-pixel lineout overplotted on the image in Fig. 98.2]. The spatial resolution and overall detector size of the CCD restrict the UVETP measurement to slightly more than one-half of the laser-beam diameter. As seen in Fig. 98.2, the laser beam is centered on the photodetector, and 560 μm of the 1010-μm (defined as the 95% enclosed energy contour) laser spot is sampled. Alignment constraints for the compilation of laser shots under consideration restrict the analysis to the central ~410 μm of the laser spot.

The amount of smoothing achieved with 1-THz, 2-D SSD and PS is quantified from the power spectrum of the measured UVETP image of Fig. 98.2. The UVETP images are Fourier transformed with a 2-D Hamming filter applied to the data, in order to obtain the power spectrum defined as the azimuthal sum at each spatial frequency of the square of the Fourier amplitudes. Good agreement is observed between the measured power spectrum for the 1-THz, 2-D SSD, and PS presented in Fig. 98.3(a) and the modeled spectrum determined

from simulated time-integrated far field. The wave number is defined as $k = 2\pi/\lambda_{SN}$, where λ_{SN} is the spatial nonuniformity wavelength, and the ℓ mode is defined as $\ell = kR$, where $R = 500$ μm is the spherical target radius. The σ_{rms} reaches 2.7% averaged over 1 ns, in agreement with the predicted 2.8%. The σ_{rms} is defined here as the square root of the ratio of the integral of power in the high frequencies (i.e., $k \geq 0.04$ μm^{-1} in the OMEGA target plane) to the integral of power in the low frequencies (i.e., $k < 0.04$ μm^{-1}). The envelope and speckle were separated at wave number 0.04 μm^{-1} in the calculation of σ_{rms} for two reasons. First, virtually all of the envelope power is contained in the first three terms of the Fourier transform, which have wave numbers $k < 0.04$ μm^{-1}; therefore, inclusion of additional terms in this sum increases the envelope power by insignificant amounts. Second, the smallest wave number of nonuniformity that can be smoothed on OMEGA with 1-THz, 2-D SSD falls between the third and fourth terms of the Fourier transform with wave numbers 0.031 and 0.046 μm^{-1}. Therefore, all the wave numbers that 2-D SSD can smooth are in the range 0.04 $\mu m^{-1} \leq k < k_c$, where $k_c = 2.7$ μm^{-1} is the cutoff wave number. The birefringent wedge was removed from the beamline, and another UVETP image was recorded to quantify the amount of smoothing
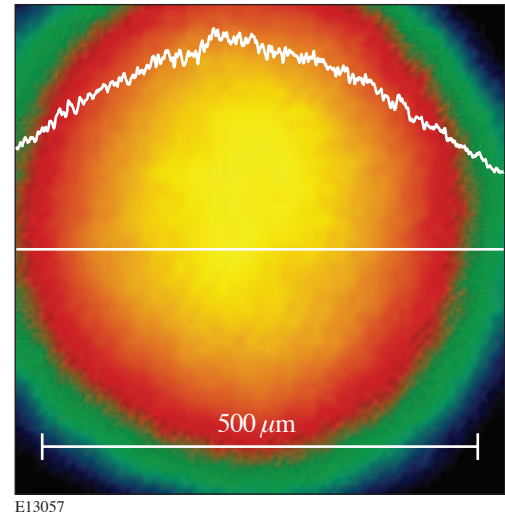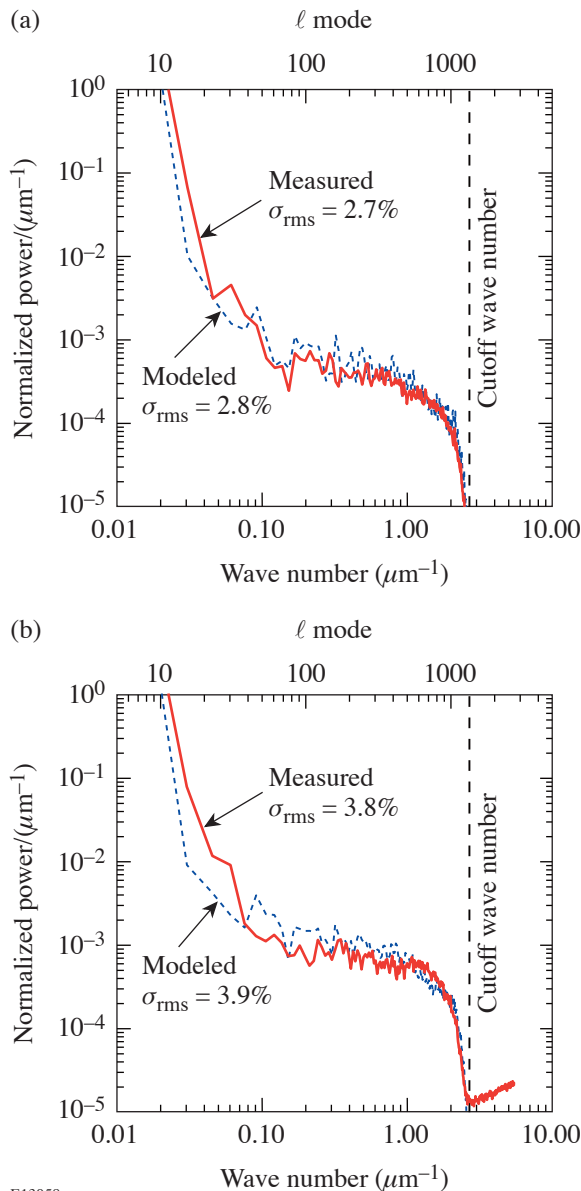

E13057

Figure 98.2
Measured UVETP image of a 1-ns square laser pulse with 1-THz, 2-D SSD and PS (shot 22835). As demonstrated with the single-pixel lineout through the center of the beam, the laser beam has a smooth spatial-intensity envelope. The spatial resolution and overall detector size of the CCD restrict the UVETP measurement to slightly more than one-half of the laser-beam profile. The laser beam is centered nominally on the photodetector, and 560 μm of the 1010-μm laser spot (defined as the 95% enclosed energy contour) is sampled.

achieved with 1-THz, 2-D SSD alone (i.e., no PS). Again, good agreement is shown in Fig. 98.3(b) between the measured power spectrum and the simulation with the expected $\sqrt{2}$ increase in σ_{rms} observed.

(a) ℓ mode

Measured $\sigma_{rms} = 2.7\%$

Modeled $\sigma_{rms} = 2.8\%$

(b) ℓ mode

Measured $\sigma_{rms} = 3.8\%$

Modeled $\sigma_{rms} = 3.9\%$

E13058

Figure 98.3
Power spectra calculated from UVETP images of (a) 1-ns square laser pulse with 1-THz, 2-D SSD and PS (shot 22835) and (b) 1-ns square laser pulse with 1-THz, 2-D SSD and no PS (shot 18249). The wave number is defined as $k = 2\pi/\lambda_{SN}$, where λ_{SN} is the spatial nonuniformity wavelength, and the ℓ mode is defined as $\ell = kR$, where $R = 500$ μm is the spherical target radius. The solid lines represent the measured power spectra; the dashed lines represent the simulations, which are in agreement with the measured results.

The measured σ_{rms} with 1-THz, 2-D SSD was also examined using 0.4-, 1.0-, and 3.0-ns square laser pulses. As shown in Fig. 98.1, the 1-THz, 2-D SSD model [Eq. (1)] is in agreement with the measured results. A more-extensive study of the smoothing rates for 0.2-THz, 2-D SSD was reported in Ref. 14, where it was shown with laser pulses having constant peak power and pulse lengths ranging from 100 ps to 3.5 ns, that the reduction in laser-irradiation nonuniformity is dependent on the spatial nonuniformity wavelength. The measured σ_{rms} for 0.2-THz, 2-D SSD is also plotted in Fig. 98.1 for comparison with the 1-THz, 2-D SSD results. As can be seen in Fig. 98.1 for the time $t \gg t_c$, but prior to reaching asymptotic levels, the measured σ_{rms} is reduced by $\sqrt{5}$ when $\Delta\nu_{UV}$ is increased from 0.2 THz to 1 THz, and it is further reduced by $\sqrt{2}$ with PS. On OMEGA, beam overlap provides an additional $\sqrt{10}$ reduction in the nonuniformity on target; therefore, with perfect energy balance and timing of the laser beams, a $\sigma_{rms} \sim 1\%$ can be achieved on target with 1-THz, 2-D SSD and PS in a few hundred picoseconds.

Conclusion

Direct-drive ICF experiments require a laser system with excellent irradiation uniformity. Laser-beam nonuniformities can be significantly reduced for high-power/energy glass lasers using 1-THz, 2-D SSD and PS. UVETP images of a single OMEGA laser beam were recorded to quantify the single-beam irradiation nonuniformity. The amount of smoothing achieved with 1-THZ, 2-D SSD and PS was determined by analyzing the power spectra of measured UVETP images of square laser pulses of varying duration. Simulated power spectra are in excellent agreement with the experimental data and permit confident extrapolation to MJ-class laser systems.

REFERENCES

1. S. E. Bodner, D. G. Colombant, J. H. Gardner, R. H. Lehmberg, S. P. Obenschain, L. Phillips, A. J. Schmitt, J. D. Sethian, R. L. McCrory, W. Seka, C. P. Verdon, J. P. Knauer, B. B. Afeyan, and H. T. Powell, Phys. Plasmas **5**, 1901 (1998).

2. J. D. Lindl, *Inertial Confinement Fusion: The Quest for Ignition and Energy Gain Using Indirect Drive* (Springer-Verlag, New York, 1998).

3. D. K. Bradley, J. A. Delettrez, and C. P. Verdon, Phys. Rev. Lett. **68**, 2774 (1992).

4. J. Delettrez, D. K. Bradley, and C. P. Verdon, Phys. Plasmas **1**, 2342 (1994).

5. J. D. Kilkenny, S. G. Glendinning, S. W. Haan, B. A. Hammel, J. D. Lindl, D. Munro, B. A. Remington, S. V. Weber, J. P. Knauer, and C. P. Verdon, Phys. Plasmas **1**, 1379 (1994).

6. R. Epstein, J. Appl. Phys. **82**, 2123 (1997).

7. V. A. Smalyuk, T. R. Boehly, D. K. Bradley, V. N. Goncharov, J. A. Delettrez, J. P. Knauer, D. D. Meyerhofer, D. Oron, and D. Shvarts, Phys. Rev. Lett. **81**, 5342 (1998).

8. V. N. Goncharov, J. P. Knauer, P. W. McKenty, P. B. Radha, T. C. Sangster, S. Skupsky, R. Betti, R. L. McCrory, and D. D. Meyerhofer, Phys. Plasmas **10**, 1906 (2003).

9. S. P. Regan, J. A. Delettrez, V. N. Goncharov, F. J. Marshall, J. M. Soures, V. A. Smalyuk, P. B. Radha, B. Yaakobi, R. Epstein, V. Yu. Glebov, P. A. Jaanimagi, D. D. Meyerhofer, T. C. Sangster, W. Seka, S. Skupsky, C. Stoeckl, D. A. Haynes, Jr., J. A. Frenje, C. K. Li, R. D. Petrasso, and F. H. Séguin, "Dependence of Shell Mix on Feedthrough in Direct-Drive Inertial Confinement Fusion," to be published in Physical Review Letters.

10. S. Skupsky and R. S. Craxton, Phys. Plasmas **6**, 2157 (1999).

11. T. R. Boehly, D. L. Brown, R. S. Craxton, R. L. Keck, J. P. Knauer, J. H. Kelly, T. J. Kessler, S. A. Kumpan, S. J. Loucks, S. A. Letzring, F. J. Marshall, R. L. McCrory, S. F. B. Morse, W. Seka, J. M. Soures, and C. P. Verdon, Opt. Commun. **133**, 495 (1997).

12. S. Skupsky, R. W. Short, T. Kessler, R. S. Craxton, S. Letzring, and J. M. Soures, J. Appl. Phys. **66**, 3456 (1989).

13. J. E. Rothenberg, J. Opt. Soc. Am. B **14**, 1664 (1997).

14. S. P. Regan, J. A. Marozas, J. H. Kelly, T. R. Boehly, W. R. Donaldson, P. A. Jaanimagi, R. L. Keck, T. J. Kessler, D. D. Meyerhofer, W. Seka, S. Skupsky, and V. A. Smalyuk, J. Opt. Soc. Am. B **17**, 1483 (2000).

15. T. J. Kessler, Y. Lin, J. J. Armstrong, and B. Velazquez, in *Laser Coherence Control: Technology and Applications*, edited by H. T. Powell and T. J. Kessler (SPIE, Bellingham, WA, 1993), Vol. 1870, pp. 95–104.

16. Y. Lin, T. J. Kessler, and G. N. Lawrence, Opt. Lett. **21**, 1703 (1996).

17. Y. Kato, unpublished notes from work at LLE, 1984; K. Tsubakimoto *et al.*, Opt. Commun. **91**, 9 (1992); K. Tsubakimoto *et al.*, Opt. Commun. **103**, 185 (1993).

18. Laboratory for Laser Energetics LLE Review **45**, 1, NTIS document No. DOE/DP40200-149 (1990). Copies may be obtained from the National Technical Information Service, Springfield, VA 22161; T. E. Gunderman, J.-C. Lee, T. J. Kessler, S. D. Jacobs, D. J. Smith, and S. Skupsky, in *Conference on Lasers and Electro-Optics*, Vol. 7, 1990 OSA Technical Digest Series (Optical Society of America, Washington, DC, 1990), p. 354.

19. T. R. Boehly, V. A. Smalyuk, D. D. Meyerhofer, J. P. Knauer, D. K. Bradley, R. S. Craxton, M. J. Guardalben, S. Skupsky, and T. J. Kessler, J. Appl. Phys. **85**, 3444 (1999).

20. F. J. Marshall, J. A. Delettrez, R. Epstein, R. Forties, R. L. Keck, J. H. Kelly, P. W. McKenty, S. P. Regan, and L. J. Waxer, Phys. Plasmas **11**, 251 (2004).

21. P. W. McKenty, T. C. Sangster, M. Alexander, R. Betti, R. S. Craxton, J. A. Delettrez, L. Elasky, R. Epstein, A. Frank, V. Yu. Glebov, V. N. Goncharov, D. R. Harding, S. Jin, J. P. Knauer, R. L. Keck, S. J. Loucks, L. D. Lund, R. L. McCrory, F. J. Marshall, D. D. Meyerhofer, S. P. Regan, P. B. Radha, S. Roberts, W. Seka, S. Skupsky, V. A. Smalyuk, J. M. Soures, K. A. Thorp, M. Wozniak, J. A. Frenje, C. K. Li, R. D. Petrasso, F. H. Séguin, K. A. Fletcher, S. Padalino, C. Freeman, N. Izumi, J. A. Koch, R. A. Lerche, M. J. Moran, T. W. Phillips, G. J. Schmid, and C. Sorce, "Direct-Drive Cryogenic Target Implosion Performance on OMEGA," to be published in Physics of Plasmas.

22. J. Paisner *et al.*, Laser Focus World **30**, 75 (1994).

23. J. E. Rothenberg, in *Solid State Lasers for Application to Inertial Confinement Fusion*, edited by W. F. Krupke (SPIE, Bellingham, WA, 1995), Vol. 2633, pp. 634–644.

24. J. A. Marozas, S. P. Regan, J. H. Kelly, D. D. Meyerhofer, W. Seka, and S. Skupsky, J. Opt. Soc. Am. B **19**, 7 (2002).